Journal of Alloys and Compounds 512 (2012) 132–139

Contents lists available at SciVerse ScienceDirect

Journal of Alloys and Compounds

journal homepage: www.elsevier.com/locate/jallcom

Complex impedance analysis of $(Y_2O_3 + CeO_2)$–$YCr_{0.5}Mn_{0.5}O_3$ composite NTC ceramics

Bo Zhang[a,b,c], Qing Zhao[a,c], Aimin Chang[a,c,*], Jincheng Yao[a,c], Pengjun Zhao[a,b,c], Fang Guan[a,b,c], Wenwen Kong[a,b,c]

[a] Xinjiang Technical Institute of Physics and Chemistry, CAS, Urumqi 830011, PR China
[b] Graduate School of the Chinese Academy of Sciences, Beijing 100049, PR China
[c] Xinjiang Key Laboratory of Electronic Information Materials and Devices, Urumqi 830011, PR China

ARTICLE INFO

Article history:
Received 2 August 2011
Received in revised form
15 September 2011
Accepted 16 September 2011
Available online 21 September 2011

Keywords:
Impedance analysis
NTC thermistors
Grain boundary

ABSTRACT

Ceramic compositions based on $(aY_2O_3 + bCeO_2)$–$0.4YCr_{0.5}Mn_{0.5}O_3$ $(a + b = 0.6)$ were prepared by conventional solid state reaction at 1200 °C, and sintered under air atmosphere at 1600 °C. For $0 \leq a < 0.6$, XRD patterns have shown that the major phases presented in the calcined powders are Y_2O_3, CeO_2 and orthorhombic perovskite $YCr_{0.5}Mn_{0.5}O_3$ phase, respectively. SEM and EDAX observations confirm the $YCr_{0.5}Mn_{0.5}O_3$ phases mostly exist at the grain, whereas the Y_2O_3 and CeO_2 phases mainly exist at the grain boundaries. Complex impedance analysis shows that, for $0 < a \leq 0.6$, single semicircular arc whose shape does not show any change with temperature. Nevertheless, for $a = 0$, two overlapping semicircular arcs are observed at and above 300 °C. The grain boundary properties exhibit thermistor parameters with a negative temperature coefficient characteristic. The relaxation behavior and conduction for the grain boundary could be due to a space-charge relaxation mechanism and oxygen vacancies, respectively.

1. Introduction

There is an increasing need for sensors for high temperature applications, such as exhaust gas and catalytic converter temperature sensing [1,2]. Such components may be negative temperature coefficient (NTC) ceramic resistors. NTC thermistors are thermally sensitive resistors whose resistance decreases with increasing temperature. They are widely used in various industrial and domestic applications, e.g., elements for the suppression of in-rush current, for temperature measurements and controls, and for compensation for other circuit elements [3].

Classical NTC thermistor ceramics composed of spinel structure (MMn_2O_4, where M = Ni, Co, Fe, Cu, Zn) show aging of the electrical properties and their application is commonly limited to temperatures below 300 °C. Rare earth (Sm, Tb, Y, etc.) perovskite oxides (ABO_3) can be used for measures at high temperature. The conduction of such oxides is dependent on the atmosphere (pO_2) and densification [4]. Ismailzade et al. [5] have reported the relationship between structure and electrical property for $Y(Cr_{1-x}Mn_x)O_3$. This composite system has the $Y(Cr_{1-x}Mn_x)O_3$ phase as a semiconducting low resistive phase, and Y_2O_3 is an insulator phase. Houivet et al. [6] have studied the composition $aY_2O_3 - bYCr_{0.5}Mn_{0.5}O_3$ $(a + b = 1)$ and have shown that, the microstructure is two-phased, compound of a Y_2O_3 phase and an orthorhombic perovskite $YCr_{0.5}Mn_{0.5}O_3$ phase. Such ceramics, with $0.5 < a < 0.7$, can be used to fabricate small NTC thermistors with a resistance value ranging from some hundreds KΩ at room temperature to some Ω at 1000 °C. In polycrystalline materials the resistive and dielectric properties usually consist of several components, such as electrode–sample interface, grain boundary and intrinsic bulk contributions, which can be separated and quantitatively determined in terms of their resistivity and capacity by alternating current (AC) impedance spectroscopy (IS) measurements [7]. The complex impedance analysis is extremely useful, particularly in differentiating the transport characteristics in grain boundaries [8]. Fujiwara et al. [2] have investigated the high temperature pO_2 stability of the composite NTC Y_2O_3–$Y(Cr_{1-x}Mn_x)O_3$. Through an impedance analysis it is determined that the increase in resistance is associated primarily with a grain boundary resistance increase.

In the present work, in order to understand the contribution of grain and grain boundaries observed in structural characterisation, the effects of temperature and frequency on $(Y_2O_3 + CeO_2)$–$YCr_{0.5}Mn_{0.5}O_3$ are investigated.

2. Experimental procedures

Ceramic compositions based on $(aY_2O_3 + bCeO_2)$–$0.4YCr_{0.5}Mn_{0.5}O_3$ were prepared via a conventional solid-state reaction method, with $a = 0$, 0.3, 0.4, 0.45, 0.5,

* Corresponding author at: Xinjiang Technical Institute of Physics and Chemistry, CAS, Urumqi 830011, PR China. Tel.: +86 991 3817189; fax: +86 991 3837510.
E-mail address: changam@ms.xjb.ac.cn (A. Chang).

0925-8388/$ – see front matter © 2011 Elsevier B.V. All rights reserved.
doi:10.1016/j.jallcom.2011.09.048

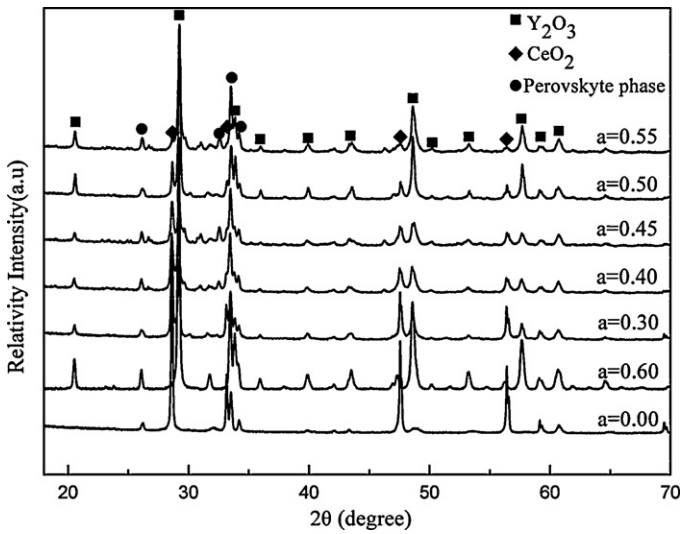

Fig. 1. XRD patterns of compositions ($aY_2O_3 + bCeO_2$)–0.4 $YCr_{0.5}Mn_{0.5}O_3$ calcined at 1200 °C.

0.55, 0.6 ($a + b = 0.6$). Powders of Y_2O_3 (analytical grade), MnO_2 (purity > 99.3%), Cr_2O_3 (purity > 99.00%), CeO_2 (analytical grade) were weighed in appropriate proportions. The weighed powders were milled in an agate mortar for 8 h to have a homogenized powder mixture. The mixture was calcined in an alumina crucible at 1200 °C for 2 h. The calcined powders were remilled in mortar for 6 h and passed through a 250-mesh sieve. Subsequently, the powders were pressed into a disk shape of 15 mm in diameter and 3 mm in thickness with a uniaxial press at 20 MPa. Cold isostatic pressing at 350 MPa was used to enhance the green densities. The pressed green disks were sintered at 1600 °C for 5 h in ambient air atmosphere.

X-ray diffractometer (XRD; BRUKERD8-ADVANCE) using CuK_α radiation was used to identify crystalline phases in calcined powders. The microstructure and phases compositions of sintered samples were observed by the scanning electron microscope (SEM; LEO1430VP, Germany) in combination with energy dispersive spectroscopy (EDS). To obtain the electrical properties, disk-shaped thermistors were designed using the in situ lead-wire attachment method (ISAM) [9,10]. A celluloid board with a height of 1.0 mm was drilled with a row of holes with diameters of about 3.0 mm, and the distance between the two holes is 1 mm. Then it was grooved on both sides of the centers of holes, and the distance between the two grooves with depths of 0.5 mm and widths of 0.1 mm is 1 mm. Two platinum lead wires (0.1 mm diameter) were placed into the two grooves. The calcined powders with starch organic binder were placed in the holes and cold-pressed to form green bodies. The celluloid board with the green bodies was heated in air to 400 °C and at that temperature for 2 h for adequate binder burnout. After the binder burnout heat treatment, the green bodies were sintered at 1600 °C for 5 h in ambient air atmosphere. The sintered samples were cut and were measured using a impedance analyzer (HP41494A) controlled by a personal computer over frequencies range from 100 Hz to 40 MHz, in a temperature range of 200–500 °C to obtain the impedance data.

3. Results and discussion

3.1. XRD and structure

Fig. 1 shows the XRD patterns of compositions ($aY_2O_3 + bCeO_2$)–0.4$YCr_{0.5}Mn_{0.5}O_3$ calcined at 1200 °C. The analysis of these diffractograms has revealed that, for $0 \le a < 0.6$, three phased ceramics. These three phases are present in different proportions in function of "a" value. They have been identified as Y_2O_3 phase, CeO_2 phase and orthorhombic perovskite phase isomorphic to $YCrO_3$ [5], respectively.

3.2. Structure and microstructure characterizations of sintered samples at 1600 °C

SEM and EDAX were employed to investigate the microstructure and compositional distributions of samples. The SEM micrographs from the surfaces of sintered samples are shown in Fig. 2. All the oxide ceramics show well grown grains in the 1–3 μm size range with almost the same morphological appearance. For a ranging from 0 to 0.55, the density of the samples becomes greater with an increase in Y_2O_3 content. A dense microstructure is necessary to consistently reproduce the electrical characteristics of the ceramics [11]. Whereas for $a = 0.6$, the microstructure of sintered samples is very porous and lowly dense. These results indicate that the CeO_2 addition increases the density. This is consistent with the previous research [12]. For $a = 0$, SEM images show a larger grain size and higher porosity than other samples. The results may be explained as follows: (1) due to a high concentration of CeO_2 phase in this composition ($a = 0$), CeO_2 acts as a sintering additive and the CeO_2 addition increases the activity of the samples by means of distortion of the lattice, resulting in an increase in the grain boundary mobility and energy, which is beneficial to grain growth in the samples; (2) the Y_2O_3 phase acting as a sintering aid can enable the production of dense ceramics [2], a low concentration of Y_2O_3 phase may lead to a decrease in density. From the above discussion, one may conclude that dense ceramics can be obtained by adjusting relative content of Y_2O_3 and CeO_2.

Microstructural observations confirm the obtaining of three-phased ceramics. The SEM image of the sample ($0.55Y_2O_3 + 0.05CeO_2$)–0.4$YCr_{0.5}Mn_{0.5}O_3$ is shown in Fig. 3(a). The compositional distributions in the grains and grain boundaries were measured using EDAX and the results are shown in Fig. 3(b) and (c). The $YCr_{0.5}Mn_{0.5}O_3$ phases mostly exist at the grain, whereas the Y_2O_3 and CeO_2 phases mainly exist at the grain boundaries.

3.3. Impedance spectrum analysis

Impedance spectrum (IS) is becoming an important analytical tool in materials research and development because it involves a relatively simple electrical measurement that can readily be automated and whose results may often be correlated with many complex materials variables: from mass transport, rates of chemical reactions, corrosion, and dielectric properties, to defects, microstructure, and compositional influences on the conductance of solids [13]. The simplified equivalent circuit configuration [14] and its impedance plane plot for polycrystalline electronic ceramic is shown in Fig. 4. The real (Z') and imaginary (Z'') parts of the impedance related to the equivalent circuit can be expressed as [8]:

$$Z' = R_g + \left(\frac{R_{gb}}{1 + R_{gb}^2 C_{gb}^2 \omega} \right), \qquad Z'' = \frac{R_{gb}^2 C_{gb} \omega}{1 + R_{gb}^2 C_{gb}^2 \omega^2}.$$

The grain resistance (R_g) and the sum of grain and grain boundaries resistance ($R_g + R_{gb}$) can be obtained from the minima of Z'' against Z'. The intersect with real axis of the semicircle at low frequencies is ascribed to the total resistance, $R_g + R_{gb}$. On the other hand, the resistance of grain (R_g) can be deduced from the left intersect of the semicircle with real axis. Fig. 5 shows the complex impedance spectrum of composite ceramics measured at various temperatures. It is observed that the area of the semicircle decreases with rise in temperature. Additionally, left intercept (R_g) shows a little change, at the same time the right intercept ($R_g + R_{gb}$) rapidly decreases with increasing temperature. These results mean that grain boundaries resistance (R_{gb}) sharply decreases with increasing temperature. The decrease in grain boundaries resistance may be caused by the increase of the thermal movement of the defects, especially the oxygen vacancies [15]. Fig. 6 shows the complex impedance spectrum of $0.6Y_2O_3$–0.4$YCr_{0.5}Mn_{0.5}O_3$ for some representative temperatures. For $a = 0.6$, the impedance spectrum (Fig. 6) has a semicircle shape, which is in good agreement with the previous research [2]. For $0 < a \le 0.6$, the impedance spectrum is characterised by the appearance of single

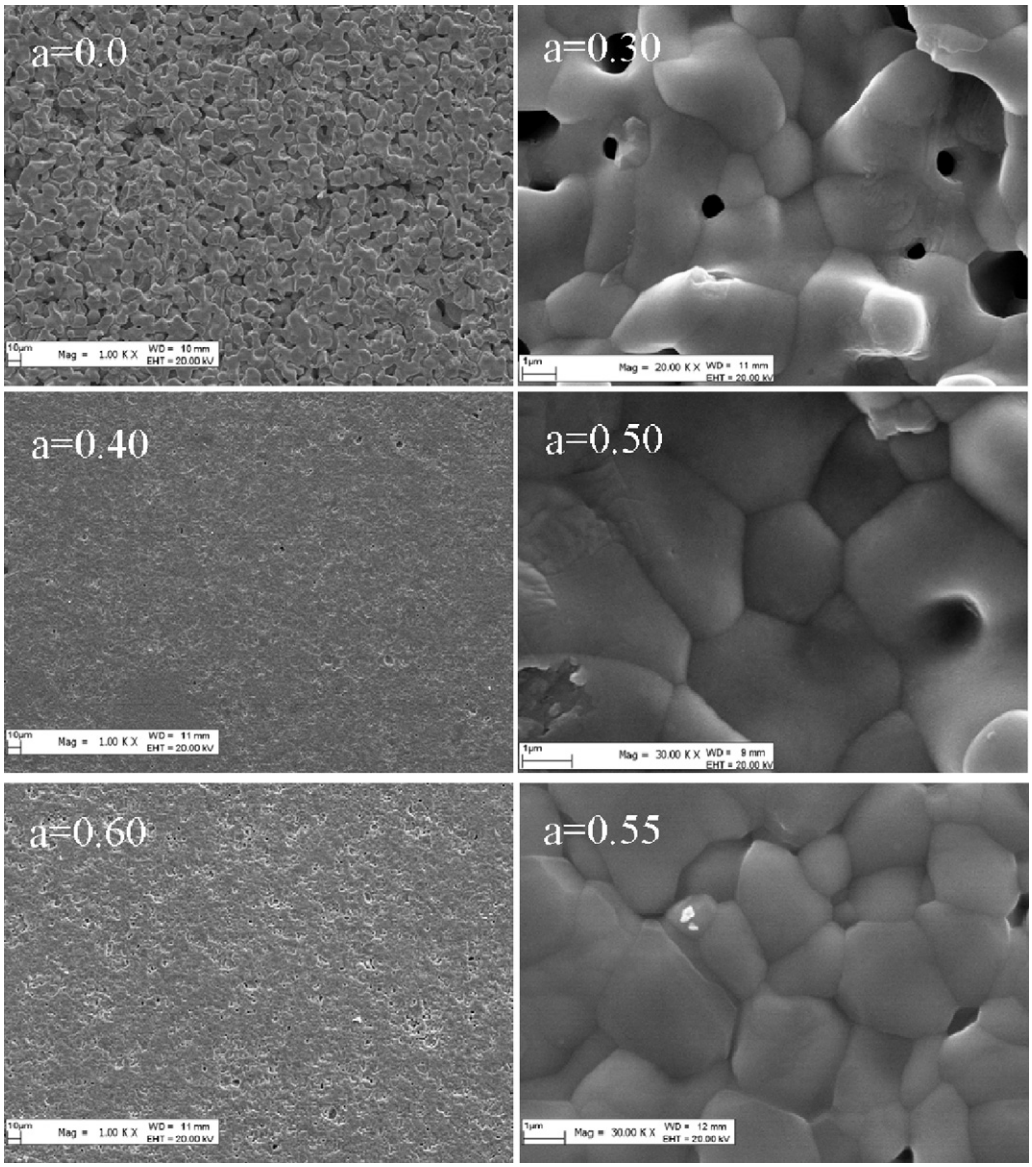

Fig. 2. SEM micrographs of sintered samples for different compositions.

semicircular arc whose radii decreases with increasing temperature. At each temperature the spectrum appears as a semi-circle diagram, the shape of which does not show any change with temperature. Nevertheless, for $a = 0$, two overlapping semicircular arcs were observed at and above 300 °C. The appearance of single semicircle in the impedance pattern at all temperatures suggests that the electrical process occurring in the material has a single relaxation process possibly due to the contribution for bulk material only [16]. The assignment of the two semicircular arcs to the electrical response due to grain interior and grain boundary is consistent with the "brick-layer model" for a polycrystalline material [17]. The complex impedance spectrum with different Y_2O_3 contents is presented in Fig. 7. At 500 °C, left intercept (R_g) shows little change, but the right intercept ($R_g + R_{gb}$) changes greatly with Y_2O_3 content. These results indicate that the magnitude of grain boundaries resistance depends on the relative content of Y_2O_3 and CeO_2. From the above discussion, the conclusion can be reached that the Y_2O_3 and CeO_2 phases mainly exist at the grain boundaries. These results have been confirmed by SEM and EDX analyses of sintered samples.

Fig. 8 shows the variation of real part of the impedance (Z') with frequency at different temperatures. The value of Z' is typically higher at lower temperatures in the low-frequency region and decreases gradually with increasing frequency. For a ranging from 0 to 0.6, the decrease in the magnitude of Z' with increasing temperature indicates an increase of ac conductivity. The Z' values merge in the high-frequency region irrespective of temperature. This result may be due to the release of space charges with rise in temperature at high frequencies. Fig. 9 shows the variation of imaginary part of the impedance (Z'') with frequency for some representative temperatures. It can be seen that Z'' reaches a maxima value at a particular frequency (relaxation frequency), which is different at different temperatures. This indicates the single relaxation process in the system [18]. The value of Z''_{max} decreases and shifts to higher frequencies with rise in temperature. These results are possibly due to the presence of space charge in the material, which is in good agreement with the observation of complex impedance data [16,19].

Fig. 10 shows the complex impedance spectrum and a fitted curve for $(0.5Y_2O_3 + 0.1CeO_2)$–$0.4YCr_{0.5}Mn_{0.5}O_3$ at different

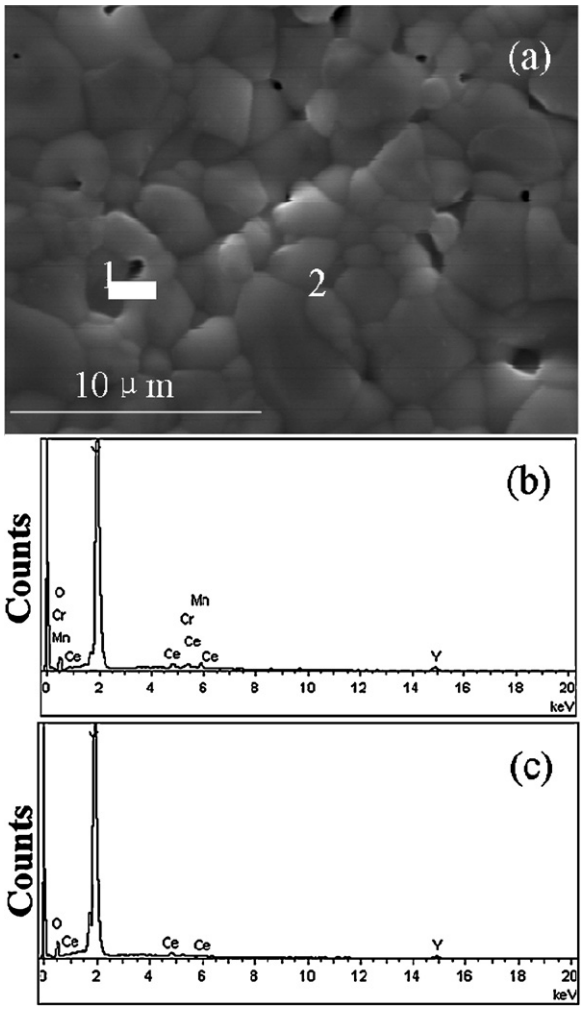

Fig. 3. SEM micrograph of the sample (a) $(0.55Y_2O_3 + 0.05CeO_2)$–$0.4YCr_{0.5}Mn_{0.5}O_3$ sintered at 1600 °C and EDS spectra; (b) grains (1) and (c) grain boundaries (2).

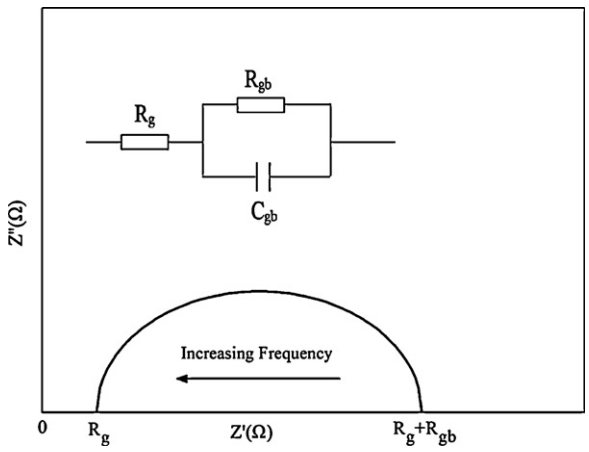

Fig. 4. Simplified equivalent circuit and impedance plane plot for polycrystalline electronic ceramic.

temperatures. The plots show a good agreement between theoretical and experimental data. The value of grain resistance (R_g) and grain boundary resistance (R_{gb}) can been obtained from the intercept of the semicircular arc on real axis (Z'). The value of relaxation frequency f_r for each temperature can be deduced from the position of the peaks in the Z''_{max} versus frequency plots (Fig. 9). And we then calculated grain boundary capacitance (C_{gb}) and relaxation time (τ) according to the relation $2\pi f_r R_{gb} C_{gb} = 1$ and $\tau = 1/\omega = 1/2\pi f_r$, respectively. Deduced values of R_g, R_{gb}, C_{gb} and τ for different temperatures are given in Table 1. The magnitude of values of the relaxation time (τ) shows that one displays a long time. This suggests that the conduction process is of the hopping type [20]. The plot of $\ln(R_{gb})$ versus $1000/T$ is presented in Fig. 11, which is well fitted by a straight line. As shown in Table 1 and Fig. 11, grain boundary resistance decreases with rise in temperature, which may be related to the negative temperature coefficient of resistance (NTCR), indicating a typical semiconducting behavior of the materials. It seems to be due to the fact that the grain boundary effect has assisted in lowering the barrier to the motion of charge carriers paving

Table 1
Electrical parameters of equivalent circuit deduced from complex impedance spectrum of composite ceramics $(aY_2O_3 + bCeO_2)$–$0.4YCr_{0.5}Mn_{0.5}O_3$ for different temperatures.

a	T (°C)	f (KHz)	R_g (Ω)	R_{gb} (Ω)	C_{gb} (nF)	τ (s)
0.00	200	57.594	381	156,660	0.0176	2.76E−06
	300	400.099	46	21,894	0.0182	3.98E−07
	400	2300.094	18	5362	0.0129	6.92E−08
	500	2800.093	16	1715	0.0331	5.68E−08
0.30	200	200.100	71	55,650	0.0143	7.95E−07
	300	1200.097	40	9791	0.0135	1.33E−07
	400	4500.089	50	2555	0.0138	3.54E−08
	500	9600.076	43	813	0.0204	1.66E−08
0.40	200	100.100	286	139,760	0.0114	1.59E−06
	300	400.099	101	36,048	0.0110	3.98E−07
	400	1100.097	36	8911	0.0162	1.45E−07
	500	4500.089	51	2853	0.0124	3.54E−08
0.45	200	200.100	89	56,084	0.0142	7.95E−07
	300	800.098	29	10,267	0.0194	1.99E−07
	400	4000.090	45	2810	0.0142	3.98E−08
	500	6500.084	78	975	0.0251	2.45E−08
0.50	200	300.099	126	48,474	0.0109	5.30E−07
	300	1500.096	36	8419	0.0126	1.06E−07
	400	5800.086	54	2219	0.0124	2.74E−08
	500	11,000.100	47	711	0.0203	1.45E−08
0.55	200	100.100	143	75,398	0.0211	1.59E−06
	300	600.099	72	17,236	0.0154	2.65E−07
	400	2300.094	44	5372	0.0129	6.92E−08
	500	5300.087	59	2116	0.0142	3.00E−08
0.60	200	117.588	203	78,949	0.0171	1.35E−06
	400	900.098	39	11,917	0.0148	1.77E−07
	500	2200.095	50	5003	0.0145	7.23E−08

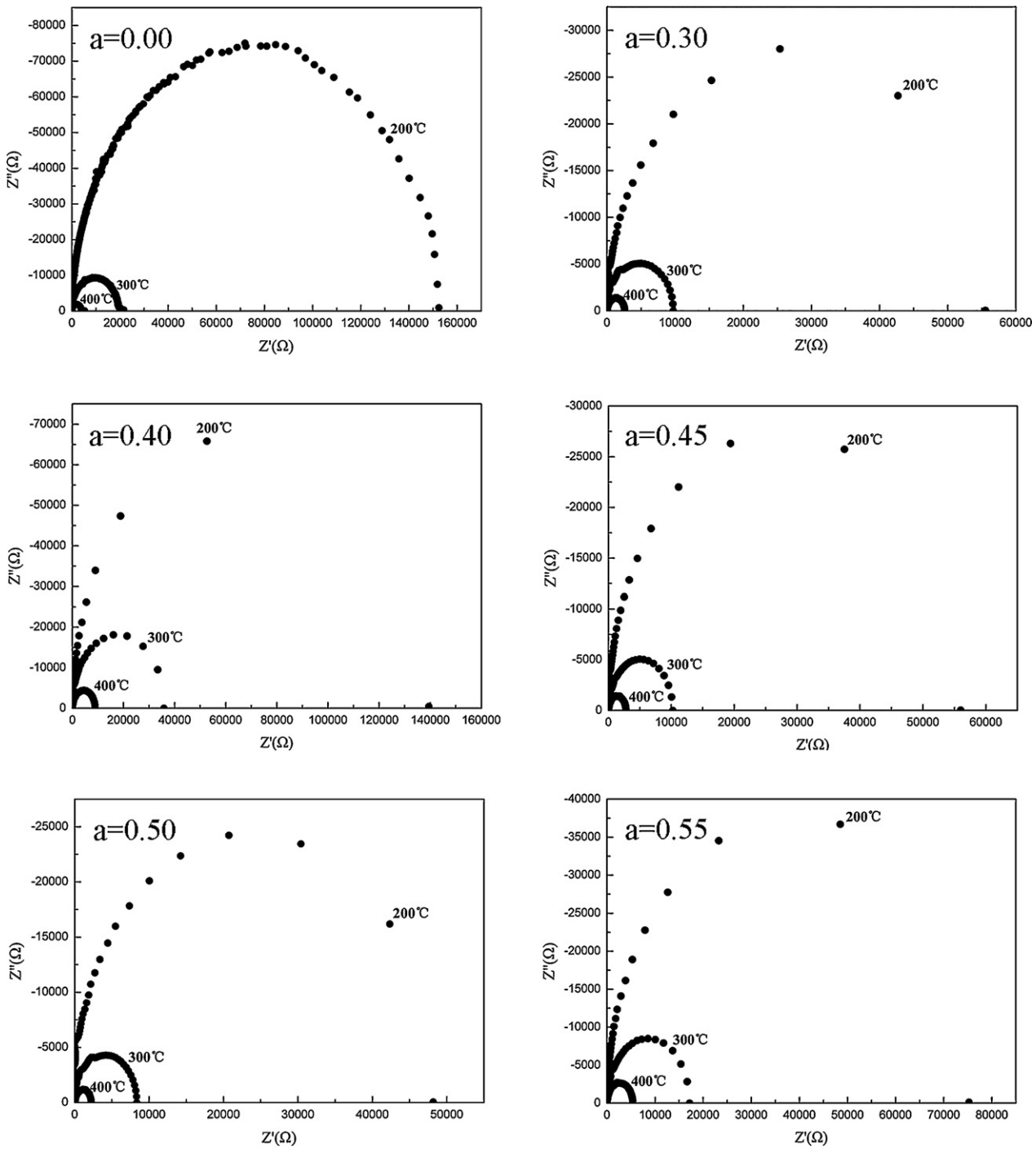

Fig. 5. The complex impedance spectrum of composite ceramics ($a$$Y_2O_3$ + $b$$CeO_2$)–0.4$YCr_{0.5}Mn_{0.5}O_3$ at various temperatures ranging from 200 to 400 °C.

the way for increased electrical transport with rise in temperature [8]. The resistance of the grain boundary follows an Arrhenius law: $R_{gb} = R_0 \exp(E_a/kT)$, where R_0 represents a pre-exponential factor and E_a, k and T are the activation energy for conduction, Boltzmann's constant and the absolute temperature, respectively [21]. The natural logarithm of grain boundary relaxation time τ_{gb}, as a function of reciprocal temperature 1000/T, is shown in Fig. 12. The derived data are well described by the Arrhenius type expression [22]: $\tau_{gb} = \tau_0 \exp(E_{a\tau}/kT)$, where τ_0 is the pre-exponential factor or characteristic relaxation time constant and $E_{a\tau}$ is the activation energy for the conduction relaxation. The values of E_a and $E_{a\tau}$ obtained from the slope of curves are given in Figs. 11 and 12, respectively. It is worth noticing that the inferred energy $E_{a\tau}$ is not equal to the activation energy E_a for the same composition. The activation energy ($E_{a\tau}$) for grain boundary relaxation is around 0.3008–0.4328 eV, and the activation energy (E_a) of grain boundary conduction is in the range of 0.2825–0.4725 eV. This phenomenon was also observed in $PbTiO_3$ doped with La [23]. The results may be attributed to a space-charge polarization in which the free carriers are stored at the two dielectric electrode interfaces [24]. As we all know, lattice-related relaxation depends on the defect lattice vibration frequency, the relaxation process observed for the grain

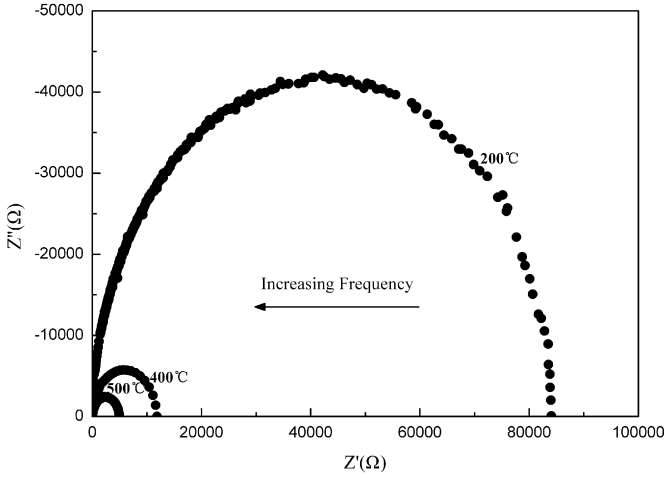

Fig. 6. The complex impedance spectrum of $0.6Y_2O_3$–$0.4YCr_{0.5}Mn_{0.5}O_3$ at different temperatures ranging from 200 to 500 °C.

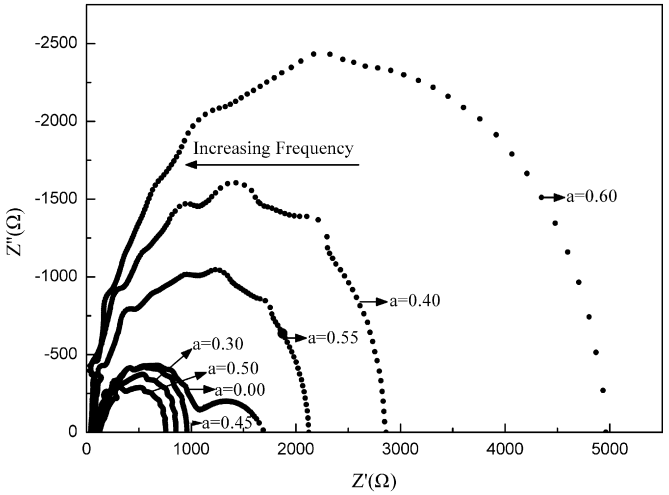

Fig. 7. The complex impedance spectrum with different Y_2O_3 contents measured at 500 °C.

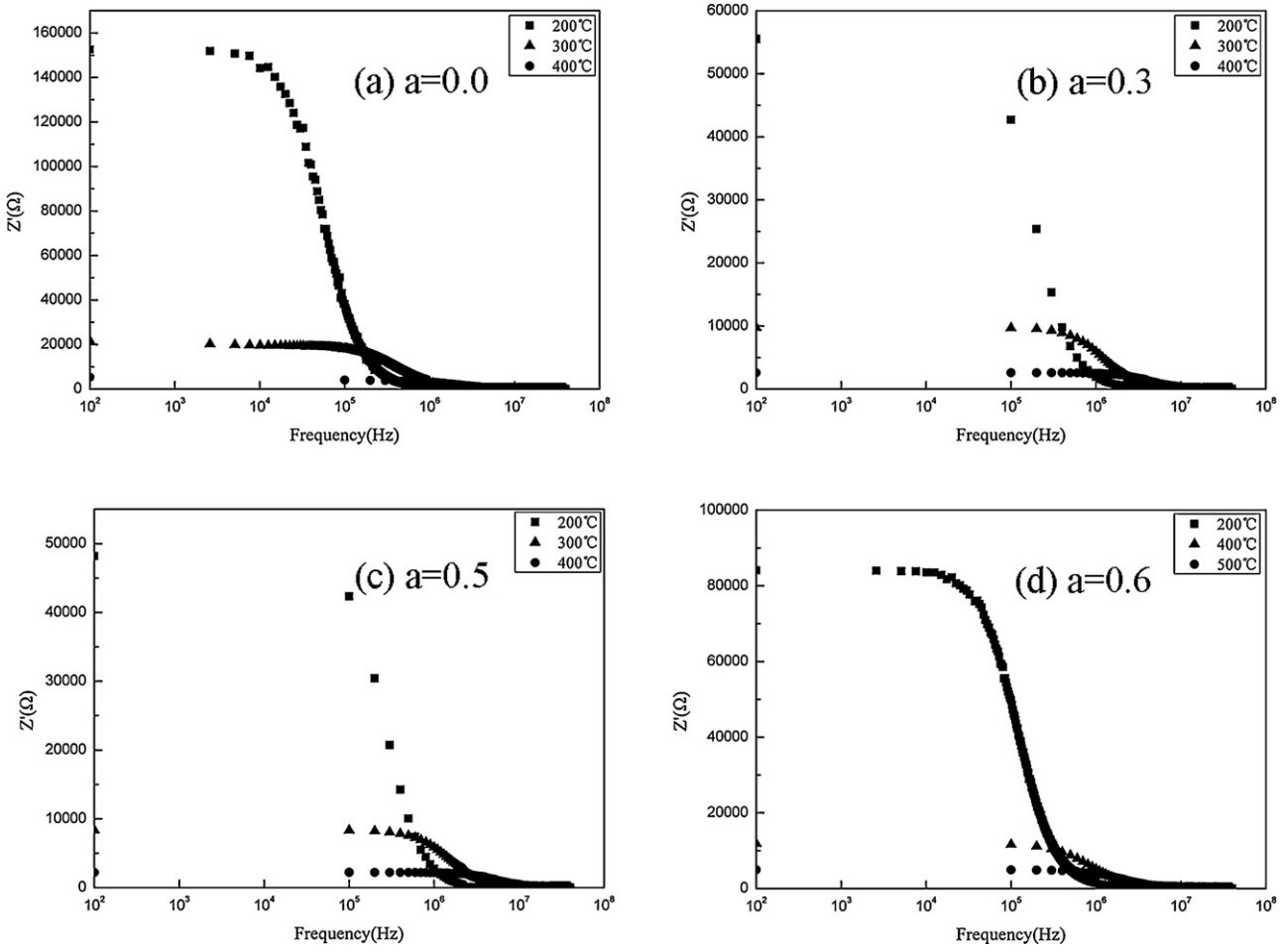

Fig. 8. Variation of real part of the impedance (Z') with frequency at different temperatures.

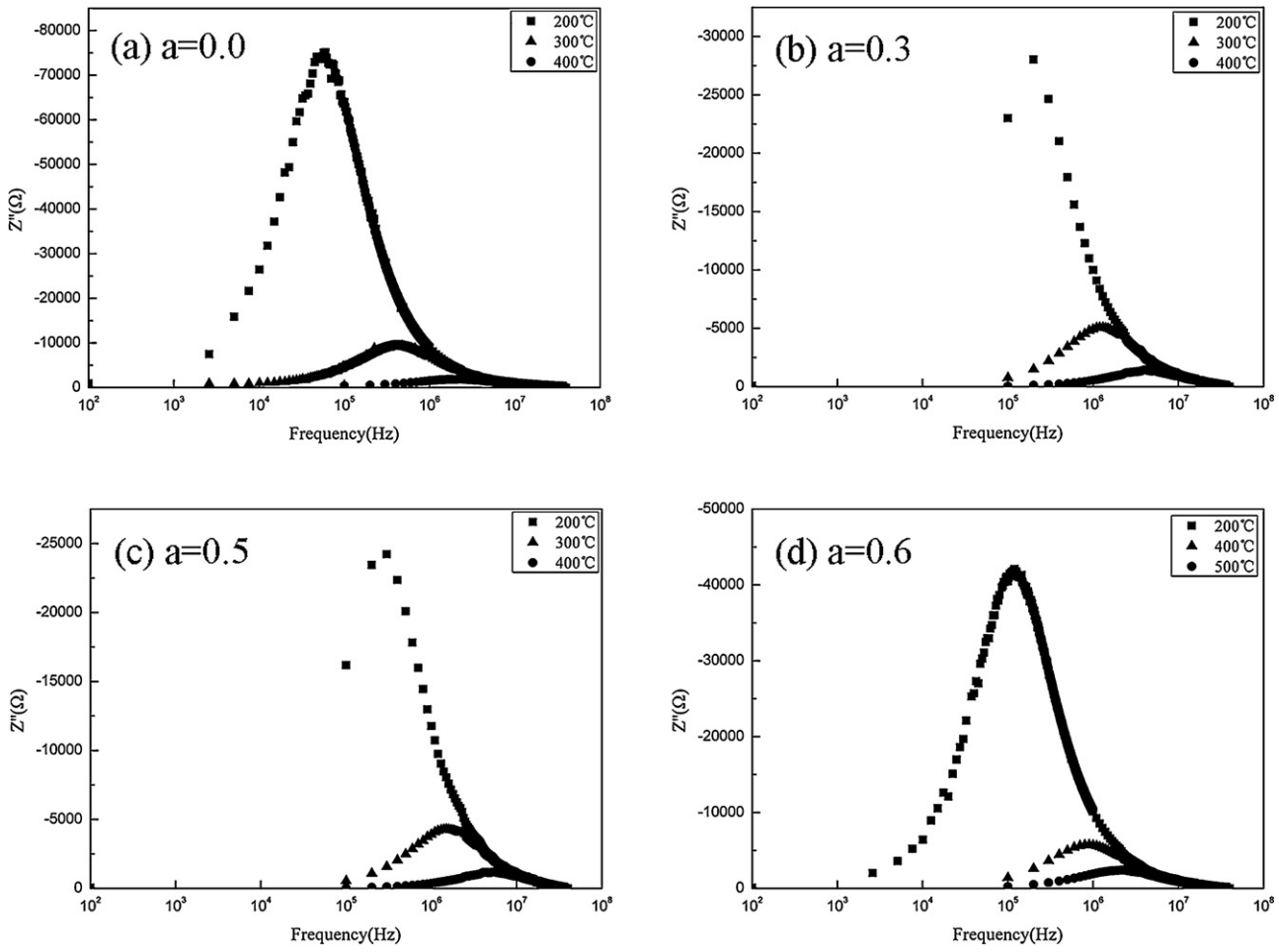

Fig. 9. Variation of imaginary part of the impedance (Z'') with frequency for some representative temperatures.

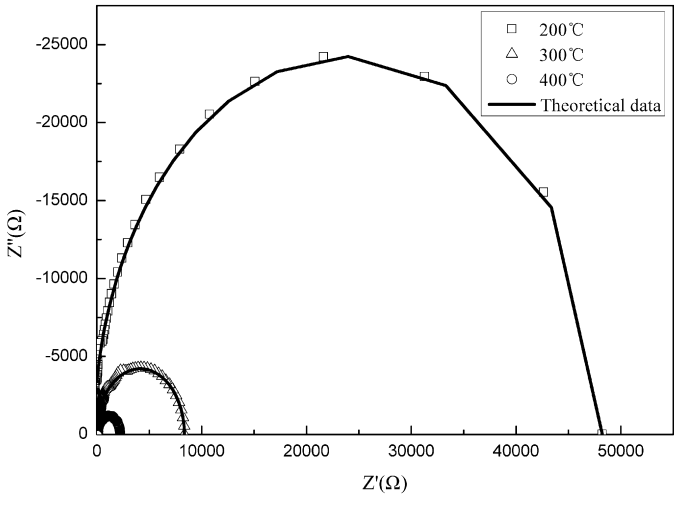

Fig. 10. Complex impedance spectrum and a fitted curve for $(0.5Y_2O_3 + 0.1CeO_2)$–$0.4YCr_{0.5}Mn_{0.5}O_3$ at different temperatures.

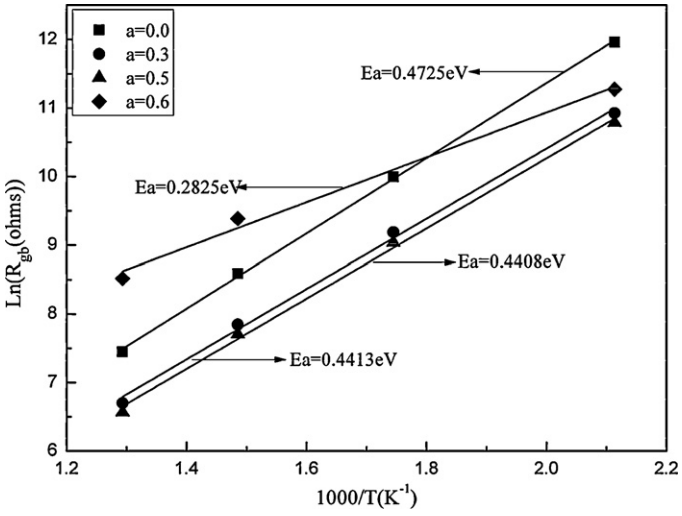

Fig. 11. Variation of $\ln(R_{gb})$ versus $(1000/T)$ of samples with different Y_2O_3 contents.

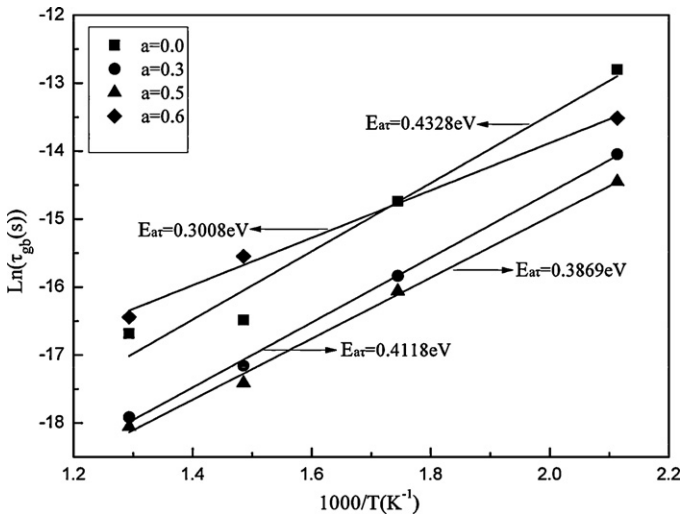

Fig. 12. Plot of the relaxation constant versus inverse of temperature for samples with different Y_2O_3 contents.

boundary region derives from a lattice defect structure. It seems that the relaxation behavior observed for the grain boundary could be ascribed to a space-charge mechanism being an intrinsic feature of grain boundary [21]. The grain boundary conduction may be due to oxygen vacancies, which may lead to the generation of hopping electrons [25].

4. Conclusion

Different compositions of $(aY_2O_3 + bCeO_2)$–$0.4YCr_{0.5}Mn_{0.5}O_3$ $(a+b=0.6)$ were prepared by conventional solid state reaction at 1200 °C, and sintered under air atmosphere at 1600 °C. For $0 \leq a < 0.6$, the major phases presented in the calcined powders are Y_2O_3, CeO_2 and orthorhombic perovskite $YCr_{0.5}Mn_{0.5}O_3$ phase, respectively. Microstructural observations confirm the $YCr_{0.5}Mn_{0.5}O_3$ phases mostly exist at the grain, whereas the Y_2O_3 and CeO_2 phases mainly exist at the grain boundaries. The dense ceramics can be obtained by adjusting relative content of Y_2O_3 and CeO_2. Complex impedance analysis shows that, for $0 < a \leq 0.6$, single semicircular arc whose shape does not show any change with temperature. Nevertheless, for $a = 0$, two overlapping semicircular arcs are observed at and above 300 °C. The grain boundary properties exhibit thermistor parameters with a negative temperature coefficient characteristic. The activation energy $(E_{a\tau})$ for grain boundary relaxation is around 0.3008–0.4328 eV, and the activation energy (E_a) of grain boundary conduction is in the range of 0.2825–0.4725 eV. The relaxation behavior and conduction for the grain boundary could be due to a space-charge relaxation mechanism and oxygen vacancies, respectively.

Acknowledgments

This study was supported by the National Natural Science Foundation of Xinjiang, CN (2010211A59), the Science & Technology Project of Urumqi, Xinjiang, CN (G08211002) and the Production Project of Economic and Informatization Commission, Xinjiang, CN (1039571301).

References

[1] A. Feteira, J. Am. Ceram. Soc. 92 (2009) 967.
[2] K. Fujiwara, S. Lee, N. Donnelly, T. Yamaguchi, C.A. Randall, J. Am. Ceram. Soc. 92 (2009) 2634.
[3] K. Park, J. Lee, S.J. Kim, W.S. Seo, W.S. Cho, C.W. Lee, S. Nahm, J. Alloys Compd. 467 (2009) 310.
[4] Y. Luo, X.Y. Liu, Mater. Lett. 59 (2005) 3881.
[5] I.H. Ismailzade, G.A. Smolenskii, V.I. Nesterenko, F.A. Agaev, Phys. Status Solidi A 5 (1971) 83.
[6] D. Houivet, J. Bernard, J.M. Haussonne, J. Eur. Ceram. Soc. 24 (2004) 1237.
[7] R. Schmidt, A.W. Brinkman, Adv. Funct. Mater. 17 (2007) 3170.
[8] H. Rahmouni, M. Nouiri, R. Jemai, N. Kallel, F. Rzigua, A. Selmi, K. Khirouni, S. Alaya, J. Magn. Magn. Mater. 316 (2007) 23.
[9] A. Banerjee, S.A. Akbar, Sens. Actuators A 87 (2000) 60.
[10] Y.Q. Lan, L.H. Yu, G.M. Chen, S.F. Yang, A.M. Chang, Int. J. Thermophys. 31 (2010) 1456.
[11] K. Park, J.K. Lee, J. Alloys Compd. 475 (2009) 513.
[12] L.B. Kong, T.S. Zhang, J. Ma, F. Boey, R.F. Zhang, J. Alloys Compd. 372 (2004) 290.
[13] J.R. Macdonald, W.B. Johnson, Fundamentals of Impedance Spectroscopy, John Wiley, New York, 1987.
[14] S.G. Song, Z. Ling, F. Placido, Mater. Res. Bull. 40 (2005) 1081.
[15] J. Jiang, T. Zhang, B. Zhang, H. Mao, J. Electroceram. 21 (2008) 258.
[16] A. Shukla, R.N.P. Choudhary, A.K. Thakur, J. Phys. Chem. Solids 70 (2009) 1401.
[17] S. Dutta, R. Choudhary, P. Sinha, A.K. Thakur, J. Appl. Phys. 96 (2004) 1607.
[18] C.K. Suman, K. Prasad, R.N.P. Choudhary, Mater. Chem. Phys. 97 (2006) 425.
[19] J. Fleig, J. Maier, J. Eur. Ceram. Soc. 24 (2004) 1343.
[20] M.A.L. Nobre, S. Lanfredi, Appl. Phys. Lett. 81 (2002) 451.
[21] M.A.L. Nobre, S. Lanfredi, J. Appl. Phys. 93 (2003) 5576.
[22] M.A.L. Nobre, S. Lanfredi, Appl. Phys. Lett. 82 (2003) 2284.
[23] O. Bidault, P. Goux, M. Kchikech, M. Belkaoumi, M. Maglione, Phys. Rev. B 49 (1994) 7868.
[24] C. Ang, Z. Yu, L.E. Cross, Phys. Rev. B 62 (2000) 228.
[25] K. Sambasiva Rao, D. Madhava Prasad, P. Murali Krishna, B. Tilak, K.C. Varadarajulu, Mater. Sci. Eng. B 133 (2006) 141.